Corrosion performance of different alloys exposed to HTL conditions—A screening study

Daniel Blücher[1] ⓘ | **Torstein Lange[1]** | **Judit Sandquist[2]** | **Inge Saanum[2]** | **Mikko Uusitalo[3]**

[1]SINTEF Industry, Trondheim, Norway

[2]SINTEF Energy Research, Trondheim, Norway

[3]Valmet Technologies, Tampere, Finland

Correspondence
Daniel Blücher, SINTEF Industry, Richard Birkelands Veg 3, 7034 Trondheim, Trøndelag, Norway.
Email: daniel.blucher@sintef.no

Funding information
European Commission, Grant/Award Number: 884111

Abstract

The corrosion and material evaluation study in (a) water-based simulated black liquor and (b) water-based simulated black liquor at super-critical conditions was successful. The conclusion from the testing program was that the most resistant alloy for the defined conditions is the chromium-rich carbon steel candidate P91 (UNS K91560). This is a type of creep strength-enhanced ferritic alloy, which is steel designed to retain strength at high temperatures. The P91 abbreviation represents the material's chemical composition, that is, 9 wt% chromium (Cr) and 1 wt% molybdenum (Mo). Further work is required to conclude the corrosion resistance for the P91 quality at supercritical conditions in the welded condition and to better understand caustic corrosion mechanisms.

KEYWORDS

aviation, black liquor, caustic corrosion, corrosion, fuel, HTL, hydrothermal liquefaction, shipping, stress corrosion cracking, super critical conditions

1 | INTRODUCTION

Black liquor is the by-product from the kraft process when digesting pulpwood into paper pulp removing lignin, hemicelluloses, and other extractives from the wood to free the cellulose fibers.[1] Black liquor is considered abundant with an annual availability of 170 million tons globally. European pulp production is forecasted to increase, with 36 Mtoe of BL generation by 2050. The chemical composition of black liquor is dependent on the source species. The inorganic part of black liquor consists of sodium sulfite, sodium thio-sulfate, sodium hydroxide, and sodium chloride, while the organic part consists of lignin and polysaccharides originating from hemicellulose and cellulose.[1] The black liquor valorization possibilities and potential are also dependent on the chemical composition. Various suggestions exist on black liquor valorization, but today it is mostly burnt in recovery boilers.

Black Liquor to Fuel (BL2F) is a European Union Horizon 2020 project (research and innovation action, Grant Agreement no. 884111) that aims to develop production technology for drop-in biofuels for aviation, transport, and shipping, using black liquor, a side stream of the chemical pulping industry as raw material. By using cost-effective and low-emission refinery processes, BL2F will help to provide solutions to the demand for more environmentally friendly fuels for aviation and shipping.[2]

Hydrothermal liquefaction (HTL), as a thermochemical biomass conversion technology, has been of interest for a long time due to its benefits compared to conventional thermal processes. The process uses sub- or supercritical water as a reaction medium and solvent at moderate temperatures (200–400°C) and high pressures (10–38 MPa).

The conversion results in the breakdown of the complex molecules found in the biomass, giving four phases, solid, gas, and liquid. The liquid phase consisting of crude and aqueous phase. The crude phase, also called bio-oil or biocrude, must be upgraded to obtain transportation fuels. The advantages of HTL are crude with high energy density, short reaction times, high efficiency, and feedstock robustness.[3]

Despite the benefits, HTL has several bottlenecks, some of them are operational issues, such as safety, fouling and clogging, pumpability of the feedstock, product quality, mechanical stress on the reactor, and corrosion. Corrosion can be classified into chemical and electrochemical corrosion forms, of which the electrochemical one is the most relevant for HTL according to Ghavami et al.[4] Corrosion of different alloys is widely studied in supercritical water reactions as it must be known to be able to design reliable and safe nuclear reactors. However, those studies consider only the supercritical water effect on the metal surfaces without the additional effect of biomass feedstock and its degradation products. The reaction chemistry in HTL is complex and demanding, it is still not fully understood. In addition, product characterization remains a challenge as liquid products are mixtures of hundreds of different compounds. HTL is carried out using a homogenous catalyst and, in some cases, H-donors to increase the biocrude yields and quality, which adds to the complexity.

To make HTL a viable industrial process, the corrosion resistance of the candidate construction materials must be known. There have been a few attempts to assess the corrosion performance of reactor alloys under simulated HTL processes. Liu et al. have studied the role of alloying elements (Cr, Fe, Ni, and Mo) on corrosion in autoclaves as well as through thermodynamic calculation in a simulated HTL environment.[5] They added inorganic corrodents (Cl^- and S^{2-}) and acetic acid to simulate the HTL conditions. The metal alloys were cut into rectangles and put into autoclaves. They have ranked the corrosion resistance as follows: P91 << SS316L < SS310 < Alloy C-276 < Alloy 625. They also found that the corrosion rates will increase with the presence of catalysts as well as increasing the ratio of acetic acid and corrodents.

In the BL2F project, the suitability of different types of alloys as reaction vessels and process component material was evaluated by testing in simulated and real process conditions with a special focus on resistance to corrosion and/or cracking. The testing program was developed and performed in the SINTEF laboratories.

The aim of this work was to expose industrially relevant construction alloys to artificial and real HTL conditions and evaluate their suitability for application in a full-scale plant.

2 | MATERIALS AND METHODS

2.1 | Material selection

A thorough selection of candidate materials was based on their potential application in a demo-scale and a potential full-scale BL2F plant and the following criteria were established for suitability:

- Industrial experience and recommendations
- Expected lifetime
- Extent of maintenance and inspection
- Availability and redundancy
- Price
- Delivery time
- Weldability
- Formability/machinability
- Mechanical properties (durability), and
- IPR/sharing/publishing aspects

Since high pH environments at supercritical conditions with aggressive organic (radical) species are not typical conditions used as a basis for the development of large volumes of corrosion-resistant alloys (CRAs), both literature research and discussions with contacts within the chemical processing industry, as well as project partners, was required.

Further, high costs for the development of brand-new alloys were a no-go criterion as it is not compatible with the expensive development of a new alternative process for drop-in fuel competing with established fossil fuels. The same applied to patented tailormade alloys available at one supplier only. Hence, well-known commercially available qualities provided by several suppliers were selected. It was also proposed to include Al-containing qualities widely used in syngas processes for the production of hydrogen, ammonia, and methanol, and reformers in the chemical and petrochemical industries. These are characterized by very good corrosion resistance in carburizing and oxidizing media as well as excellent resistance to metal dusting, high-temperature creep, and oxidation at high temperatures. The well-known pressure vessel steel quality P91 (EN 10222-2) in normalized and tempered conditions was also proposed. As a result, the following qualities were included in the corrosion assessment:

- Titanium grade 2
- Stainless steel alloy 316, SAF 2507, and 254 SMO
- Nickel-chromium-molybdenum-based alloys Inconel 625 and C276
- Nickel-chromium-aluminum alloy 602 CA and 699 XA
- The chromium-rich carbon steel P91 (X10CrMoVNb9-1)

Un-alloyed carbon steel qualities were not selected as the corrosion rate was expected to be unacceptably high, which could also result in potential problems with clogging etc. of critical process equipment as well as potential poisoning of downstream catalysts in addition to extended need for maintenance, inspection, and replacements.

A detailed presentation of the selected nine material candidates for corrosion testing is presented in Table 1.

2.2 | Production of the test specimens

Small C-ring test specimens were stressed to their respective yield strength at the test temperature, that is, compensated for high temperature de-rating for each alloy. To obtain the specific stress levels equal to the yield for the different alloys, tensile testing was conducted at the actual test temperature for each alloy and then used as a basis for the correct deflection of the C-ring specimens. The correct deflection (stress) was obtained by strain control and the use of strain gauges. The deflection stops when the target strain, corresponding to the yield strength, is achieved. The test specimens have the form of C-rings to simulate the hoop stress from the high inside pressure in the real process. Hoop stress acts perpendicular to the axial direction and is the stress that occurs along the pipe's circumference when pressure is applied. Hoop stresses are tensile and generated to resist the bursting effect that results from the application of pressure. Stress-strain curves were generated by tensile testing for the different materials at the desired test temperature to be able to stress (pre-load/deflect) the C-rings with bolts and nuts to achieve the desired yield strength on the inside of the rings. The C-ring test is NACE TM0177 method C,[6] and there is also guidance given in EFC 16[7] and EFC 17.[8] To avoid galvanic corrosion problems, the threaded rods and nuts were machined from the same material quality as the C-rings.

The C-ring test is effectively a bend/deflection test, suitable for relatively small tubulars. If the ring is compressed, a tensile stress is generated on the outside. However, as pipes usually carry an environment of concern on the inside, the ring must be expanded, producing stress in the hoop direction by opening the C-ring with the centered bolt, as shown in Figure 1.

The samples were pre-loaded to achieve the desired inside yield stress using strain control and strain gauges. Ideally, the compression on the outside shall be the same as the strain on the inside. However, this is not the case in practice, and it was therefore produced compression and corresponding strain data for all materials by use of glued strain gauges on spare specimens. Then, when a compression/strain ratio (correction factor) was found for all materials, the real specimens were deflected by

TABLE 1 Shortlisted nine potential material candidates to be tested, including alloy composition.

| Pipe/Plate no.	Marked	Grade	UNS No.	C%	Si%	Mn%	P%	S%	Cr%	Ni%	Mo%	Co%	Cu%	Al%	N%	V%	Nb%	Nb+Ta%	W%	Zr%	Y%
1	None (paper tube)	Ti grade 2	R50400	0.006											0.005						
2	Sandvik 3R60	316	S31603	0.02	0.45	1.64	0.03	0.007	17.34	13.12	2.63	0.12	0.26	0.003	0.037						
3	Sandvik SAF2507	25Cr SDSS	S32750	0.013	0.28	0.44	0.02	0.0005	25.35	6.46	3.85	0.11	0.13	0.014	0.29						
4	2X22RK69	254 SMO	S31254	0.012	0.44	0.43	0.025	0.0005	19.97	17.78	6.12	0.091	0.65	0.02	0.2						
5	EN10216-2, ASTMA3350	X10CrMoVNb9-1 P91	K94560	0.095	0.31	0.5	0.014	0.001	8.23	0.27	0.85	0.07	0.07	0.01	0.045	0.2	0.066				
6	NiCr22Mo9Nb	Alloy625 (Inconel)	N06625	0.023	0.19	0.07	0.005	0.002	21.6	61.41	8.6	0.03	0.03	0.15				3.35			
7		Alloy C276	N10276	0.003			0.005	0.003	16.07	57.01	16.14	0.46				0.19			3.44		
8	NiCroFer 6025 HT, NiCr25FeAlY	Alloy 602 CA	N06025	0.18	0.12	0.1	0.004	0.002	25.36	61.7			0.01	2.23						0.07	0.07
9	30402	Alloy 699 XA	N06699	0.2	0.05	0.01	0.002	0.002	29.6	67.8	0.01		0.01	2.2	0.017		0.14			0.03	
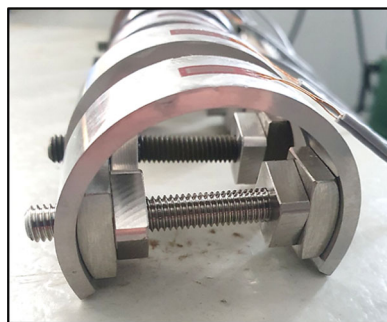
FIGURE 1 C-ring specimens with strain control attached according to NACE TM0177 method C. [Color figure can be viewed at wileyonlinelibrary.com]

placing the extensometer on the outside and the rings expanded till the target strain values (equal to yield) were achieved (see Table 2).

2.3 | Corrosion screening test of selected material candidates

The simulated water-based black liquor was designed as a standard corrosion media instead of "real" industrial black liquor to (1) act as a standardized black liquor and (2) prevent an oily protective film from forming on the sample surface originating from the lignin content. Thus, the reason for choosing a standardized water-based solution instead of real black liquor was twofold. First, black liquor is not a standard resource, it varies severely among pulp mills. Hence, the corrosion results will be conservative using a standardized solution developed in BL2F and will also cover the formation of corrosive water pockets that often form inside the tubing, tanks, and so on, in process plants. Second, it is observed that the biocrude, which is the product of interest in HTL processes, forms a protective layer (oil film) on the metal surfaces, which is expected to inhibit/reduce corrosion rates. Allowing that would require much longer tests to reveal the alloys' suitability to these conditions. By inhibiting the formation of a protective layer, it was expected that the testing time for corrosion could be greatly reduced.

A total volume of 45 L with the chosen composition (by means of weighing, see Table 3) was prepared and thereafter purged with $N_2(g)$ while simultaneously cooled.

For the initial screening testing the samples were inserted into an autoclave made of Ti grade 2 and exposed at 180°C, 200 bar for 31 days in simulated water-based black liquor at stagnant conditions. The initial pH was measured at 12.47, and the oxygen level at 2 ppb (see Table 4 and Figure 2).

The winner candidates were chosen based on the corrosion performance in the screening tests (pitting,

cracking, intergranular corrosion, general corrosion), material aspects (forming, weldability, machinability), and commercial aspects (availability, delivery time, price, redundancy of suppliers, common practice). The material and commercial aspects were revealed through interviews with the manufacturers. This evaluation gave four "winner" candidates, that is, 254SMO, P91, C276, and 699XA.

2.4 | Corrosion testing at supercritical conditions

To mimic the real conditions, the most promising alloy candidates from the screening tests were exposed to the same simulated model water-based black liquor in SINTEF's continuous HTL reactor[9] at 390°C and 300 bar. Both the C-rings and the model water-based black liquor solution were prepared new, as described previously, for this test. The C-rings were pre-loaded with strain gauges to achieve the desired inside yield strength at 390°C (see Figure 3).

The SINTEF reactor was modified to perform long-term experiments with the chosen candidates. The modifications consisted of removing the stirrer from the tank reactor and de-risking the experimental setup, where valves were mounted at the inlet and outlet of the reactor compartment to be able to turn the reactor to batch mode in case of clogging. Long-term pressure tests both cold and hot were carried out to ensure that the reactor can keep the necessary conditions even in batch mode over an extended time. Switching to batch mode is expected to have a no to minor effect on the results, as the alloys are exposed to the constant salt conditions. In addition, a sampling point for measurement of the dissolved oxygen in the water was implemented as dissolved oxygen can compromise the corrosion results.

The simulated water-based BL test was purged with $N_2(g)$ for degassing of dissolved O_2 before it was transferred to the feed tank of the HTL reactor. Eight C-rings specimens (two of each alloy) with ceramic spacers in between were placed in the reactor compartment, measuring 80 mm in diameter and 200 mm in height, and the compartment was sealed (see Figure 4). The O_2 concentration was measured in the electrolyte by a Fibox 3 LCD stand-alone fiber optic oxygen meter based on the use of a 2 mm optical in-situ fiber. The oxygen concentration was <10 ppb O_2, measured in the SINTEF reactor before start-up.

The long-term corrosion test was performed semi-continuous, continuously operating during daytime on the first days and leaving the reactor at batch conditions during nighttime. Due to clogging, the reactor was operated only in batch mode after the first week. Figure 5 shows the reactor conditions during the test, indicating that the correct

TABLE 2 Measurements of compression on the outside versus strain on the inside of C-rings by use of glued strain gauges on spare specimens to find a correlation factor for the final deflection of the test rings.

Can-didate	Sample	Target compression (μm/m) (outer)	Applied compression (μm/m)	AYS (Mpa)	Strain at AYS (%) (inner)	Outer strain gauge (μm/m)	Inner strain gauge (μm/m)	Deviation in (%) applied comp./ target comp.
Ti grade 2	1	−3074	−3052	146	0.426	−3074	4260	1%
1	2	−3074	−3074	146	0.426	−3074	4260	0%
	3	−3074	−3074	146	0.426	−3074	4260	0%
316	4	−2966	−2982	319	0.406	−2966	4060	−1%
2	5	−2966	−3005	319	0.406	−2966	4060	−1%
	6	−2966	−2977	319	0.406	−2966	4060	0%
25Cr SDSS	7	−3336	−3339	468	0.411	−3336	4111	0%
3	8	−3336	−3335	468	0.411	−3336	4111	0%
	9	−3336	−3319	468	0.411	−3336	4111	1%
254smo	10	−2532	−2549	241	0.339	−2532	3390	−1%
4	11	−2532	−2529	241	0.339	−2532	3390	0%
	12	−2532	−2525	241	0.339	−2532	3390	0%
X10CrMoVN-b9-1	13	−3143	−3175	501	0.477	−3143	4770	−1%
5	14	−3143	−3172	501	0.477	−3143	4770	−1%
	15	−3143	−3149	501	0.477	−3143	4770	0%
Alloy 625 inconel	16	−2712	−2689	369	0.374	−2712	3740	1%
6	17	−2712	−2719	369	0.374	−2712	3740	0%
	18	−2712	−2762	369	0.374	−2712	3740	−2%
C−276	19	−2489	−2485	276	0.35	−2489	3500	0%
7	20	−2489	−2477	276	0.35	−2489	3500	0%
	21	−2489	−2477	276	0.35	−2489	3500	0%
Alloy 602 CA	22	−2147	−2147	249	0.322	−2147	3220	0%
8	23	−2147	−2136	249	0.322	−2147	3220	1%
	24	−2147	−2153	249	0.322	−2147	3220	0%
Alloy 699 XA	25	−2273	−2264	232	0.313	−2273	3130	0%
9	26	−2273	−2278	232	0.313	−2273	3130	0%
	27	−2273	−2292	232	0.313	−2273	3130	−1%

Note: This was done for each material quality since they have different mechanical and de-rating properties.

TABLE 3 Model simulated water-based black liquor defined in the project.

Salt	wt% in Pristine BL	g/kg	mmol/kg
NaOH	1.2	11.8	295.1
NaHS	0.2	2.3	41.3
Na$_2$SO$_4$	1.8	17.6	124.0
Na$_2$CO$_3$	1.7	16.6	156.7
NaCl	0.1	1.4	24.2
K$_2$SO$_4$	0.6	6.4	47.5
Total	**5.62**	**56.18**	**688.79**
Sodium formate	0.5	4.9	71.8
Sodium acetate	0.3	2.5	30.8
Sodium D-gluconate	0.7	6.6	30.0
Sodium DL-lactate	0.7	7.3	65.2
Guaiacol	2.5	24.5	197.4
Total organics	**4.58**	**45.77**	**395.20**

TABLE 4 Screening test description and experimental setup with autoclave.

Description	Value
Test method	C-ring (inside in tension = hoop stress) in autoclave (Ti gr 2, 30 L)
Electrolyte composition	Standardized model composition of BL
Temperature	180°C
Pressure	200 bars
Specimens dimensions	D: 40–60 mm WT: 2–5 mm
Dissolved oxygen limit	<10 ppb (actual 2 ppb, pH 12.47)
Surface finish	Ground to SiC 500
Stress level (by strain control)	Ref. NACE (100% AYS)
Test duration	4 weeks

pressure and temperature (390°C; 300 bar) were maintained during the entire test period. The figure also indicates that there were disturbances due to clogging during the first week but at the same time, continuous operation was still possible with increased pump pressure and reduced flow.

3 | RESULTS

To narrow down the number of possible candidates for the final heat in the real HTL reactor, the least suitable candidates from the screening test were excluded from further exposure. These candidates were Ti grade 2, AISI316, 25 Cr SDSS, Inconel 625, and 602 CA, which revealed a lower corrosion performance than the rest of the candidates (see Figure 6).

Ti grade 2

Here cracking of about 100 μm of the substrate is seen as well as pitting. Since these failure modes are not acceptable in an industrial application operating at these conditions the candidate was not included in phase 2 of the study.

AISI316

The AISI316 showed about 70 μm deep pits on the tension side. Also, the side of the C-rings was covered with areas of shallow corrosion. As pitting can be the starting point of cracking, this alloy was not included in the phase 2 study.

25 Cr SDSS

This austenitic alloy revealed areas of pitting corrosion on the edges of the C-rings. Minor pitting was seen on the tension side.

Inconel 625

Also here, there was evidence of minor pitting corrosion on the tension side. Since this was found in the more benign conditions in the screening study (phase 1) this alloy was not allowed to proceed to the phase 2 exposure in "real" HTL conditions

602 CA

Interestingly, the surface of the exposed 602CA revealed a net resembling the skin of the honey melon. The aluminum in the alloy is present in the grains, which are preferentially dissolved during exposure, revealing this net-like surface appearance after exposure.

These alloys were hence not included in the final exposure to the supercritical conditions in the SINTEF HTL reactor (phase 2).

3.1 | Results from phase 2, post HTL reactor test analysis

Salt crusts were seen in the reactor causing clogging at the inlet to the reactor, in the reactor (both on the sample spacers and at the reactor bottom), and at the outlet as well, see Figure 7.

Analyzing the salt crusts with ICP-MS showed the presence of Na (from the electrolyte), Cr, Mn, Fe, Ni, Mo, W, and Al from the corroded samples and the alumina spacers, and N from the HNO$_3$ in which the salt crusts were dissolved for the analysis (Figure 7).

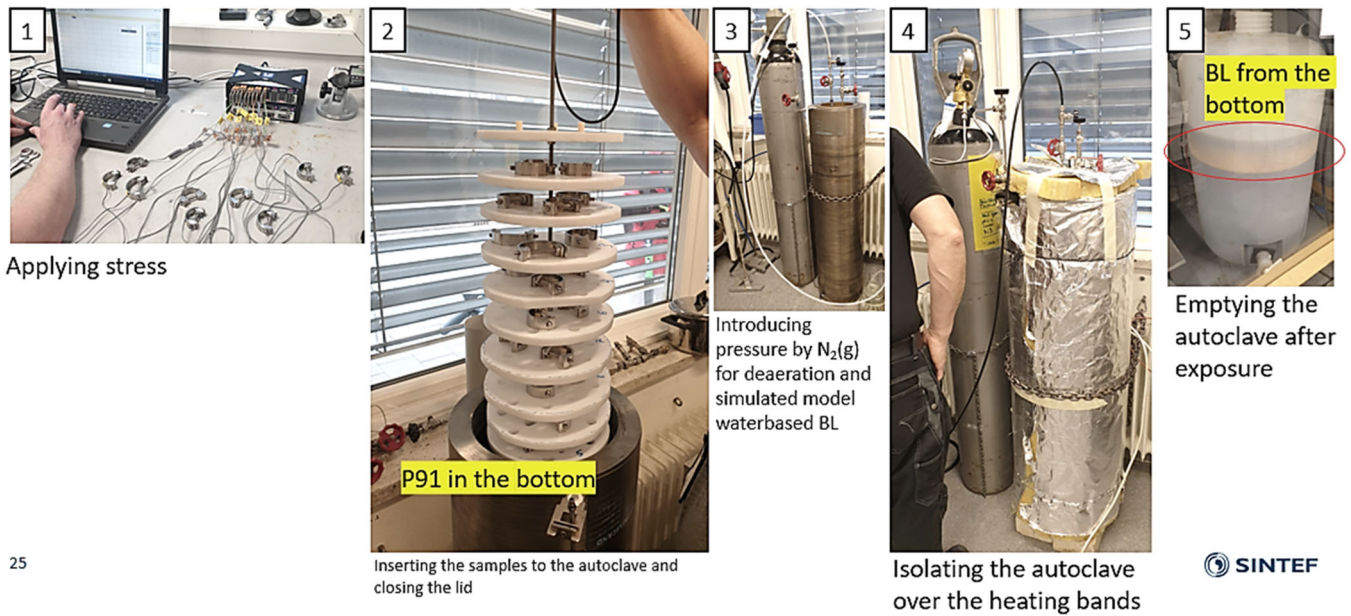The corrosion performance after the real HTL reactor testing further revealed:

FIGURE 2 Screening testing setup in autoclaves. [Color figure can be viewed at wileyonlinelibrary.com]

alloy	temp	strain at Rp02	oppspenningsfaktor inner-ytter (fra 180degC)	Outer Strain Gage (µm/m)
254smo	390	0,3341	-1,338862559	-2495
p91	390	0,4183	-1,517658288	-2756
c276	390	0,3357	-1,406187224	-2387
699xa	390	0,3118	-1,377034756	-2264
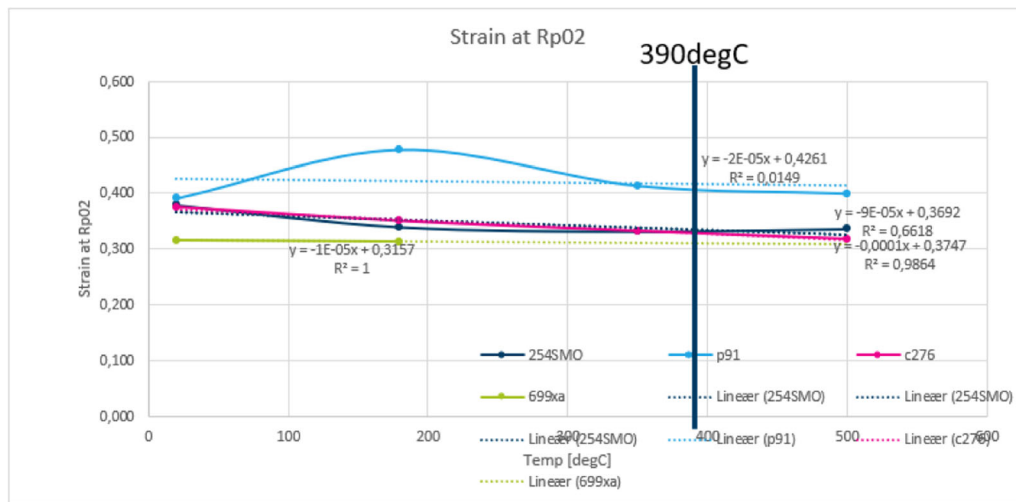
FIGURE 3 Outside compression versus inside stress at yield at 390°C (based on in-house data and extrapolation). [Color figure can be viewed at wileyonlinelibrary.com]

3.2 | 254SMO

The optical microscopy images of 254SMO as tested are seen to reveal burnt-in BL residue and salt crystals. Some cracking of the tension side indicating stress corrosion cracking (SCC) was also seen in combination with a thin layer of delaminated corroded metal (Figure 8).

The scanning electron microscopy/energy dispersive X-ray spectroscopy (SEM/EDS) analysis revealed SCC on the tension side and a delaminated oxide layer of about 2–5 µm. This layer was partly separated from the sample surface and was richer in O, Ni, and Mo compared to the substrate but lower in Fe and Cr. The Ti is most probable coming from the dissolved spacer wires, which have precipitated on the sample surface.
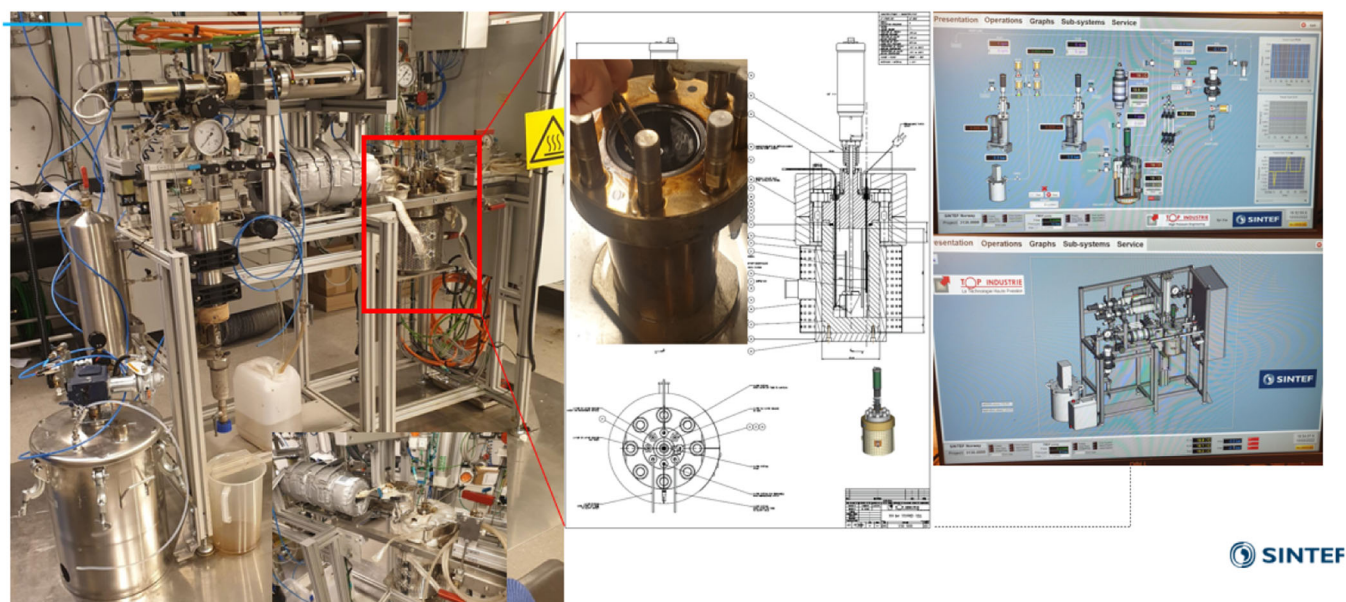
FIGURE 4 Outline of the HTL reactor operating at supercritical conditions with the C-rings inserted into the reactor compartment (upper middle image). [Color figure can be viewed at wileyonlinelibrary.com]
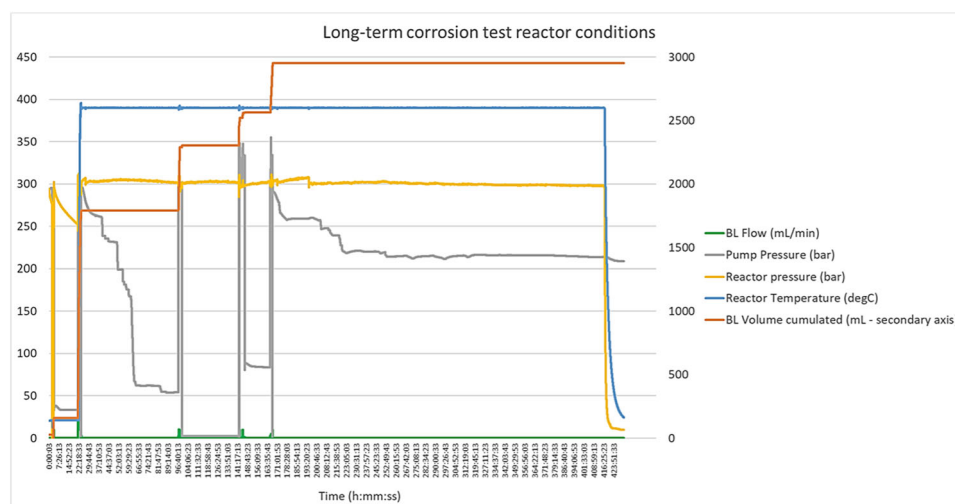
FIGURE 5 Reactor conditions during long-term corrosion tests. BL: simulated water-based black liquor. [Color figure can be viewed at wileyonlinelibrary.com]

Also, Si grains from the polishing SiC paper are seen in Figure 9.

3.3 | P91

For the P91 samples, some minor crevices and edge corrosion were seen on the nuts and hemispheres (also made of P91) used for tensioning of the C-rings. Also, residues from the BL and salt crusts were seen. However, very few signs of corrosion were evident on the stressed inside of the P91 C-rings after 18 days of exposure to the SC environment in the SINTEF-ER reactor (see Figure 12). Some minor pitting corrosion was seen in the mid-section of the C-ring (see Figure 10).

Also, the SEM/EDS analysis revealed a Fe/Cr-rich mixed oxide layer, evenly distributed on the sample surface (see Figure 11). The Si intense spot is suggested to come from the polishing of the section (SiC paper).

3.4 | C-276

For this austenitic nickel-molybdenum-chromium alloy with a small addition of tungsten, BL residues and salt crystals on the exposed surface were found. Pitting corrosion
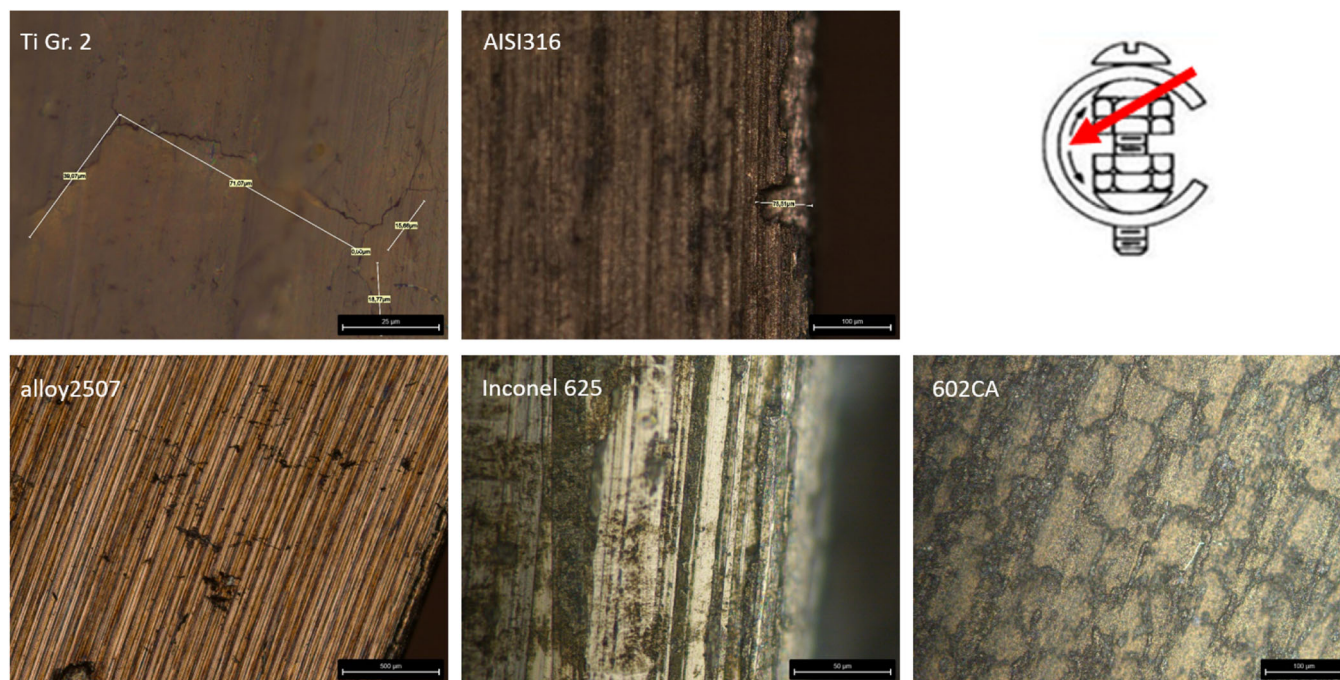
FIGURE 6 Optical microscopy images obtained from post-screening test examination of the inner, stressed edge of the C-rings as indicated by the red arrow (upper right). Candidates with insufficient corrosion resistance: Ti grade 2, AISI 316, alloy 2507, Inconel 625, and 602 CA. [Color figure can be viewed at wileyonlinelibrary.com]
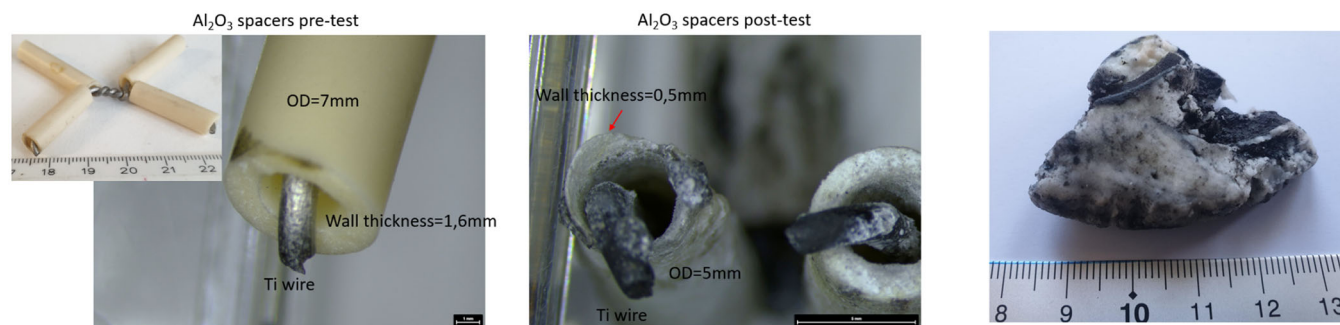
FIGURE 7 Left: Images of alumina spacers on Ti-wire suffering from dissolution in SC conditions. Right: salt crust found at the bottom of the reactor after the test. [Color figure can be viewed at wileyonlinelibrary.com]

was evident on the stressed inner edge of the C-rings and on the surface, see Figure 12. A more detailed analysis showed that also intercrystalline corrosion had taken place with the loss of occasional grains because of the applied stress in combination with corrosion.

In the SEM/EDS mapping images (Figure 13), the lost grains can be seen as black voids. The sharp sides and edges around the lost grains suggest that they have failed along the grain boundaries. Also, some SCC is seen. There is an additional layer that is rich in Cr, Mn, Fe, and Al. The Al is believed to originate from the partly dissolved alumina spacers. Unfortunately, the oxygen signal here was not mapped. However, by mapping an

adjacent area, the layer was seen to also contain oxygen, indicating that this is a corrosion layer.

3.5 | 699XA

The as-tested 699XA NiCr alloy is just like the other three candidates seen to have BL residues left on the surface after testing in the HTL reactor at SC conditions. Also here, salt crystals are present. A general corrosion attack is evident on the edge of the tension side of the exposed C-rings (see Figure 14). SCC and lost grains are seen on the tension side of the 699XA section after exposure to SC conditions.
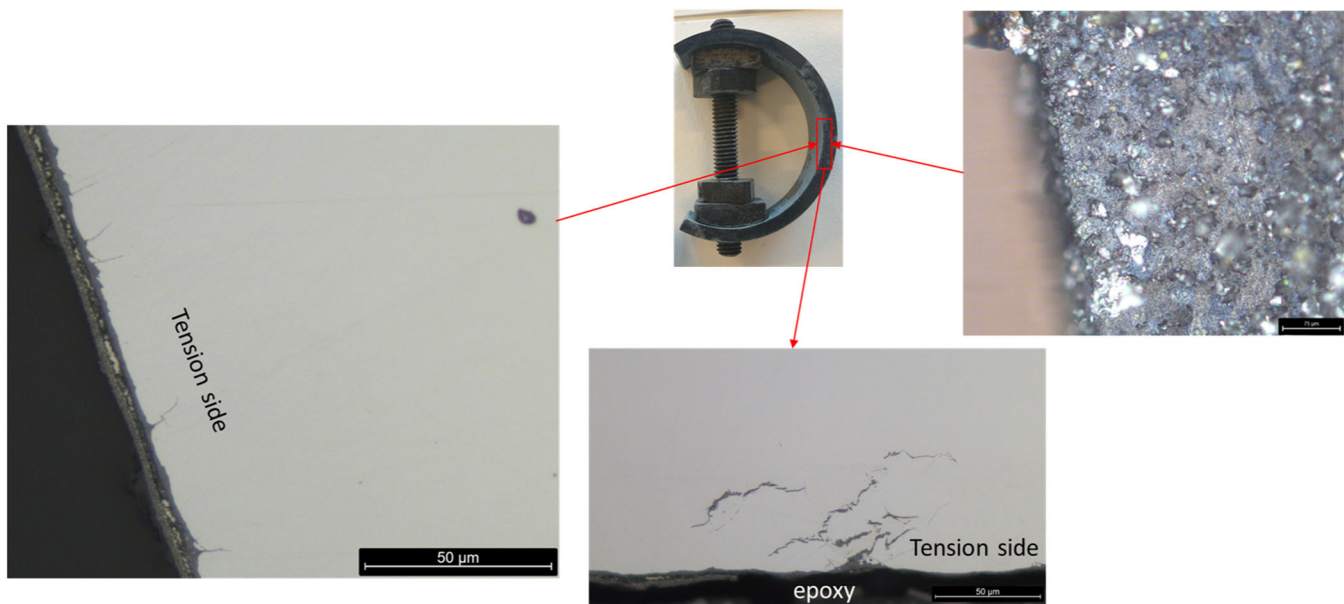
FIGURE 8 Posttest analysis of 254SMO by optical imaging of tension side. [Color figure can be viewed at wileyonlinelibrary.com]
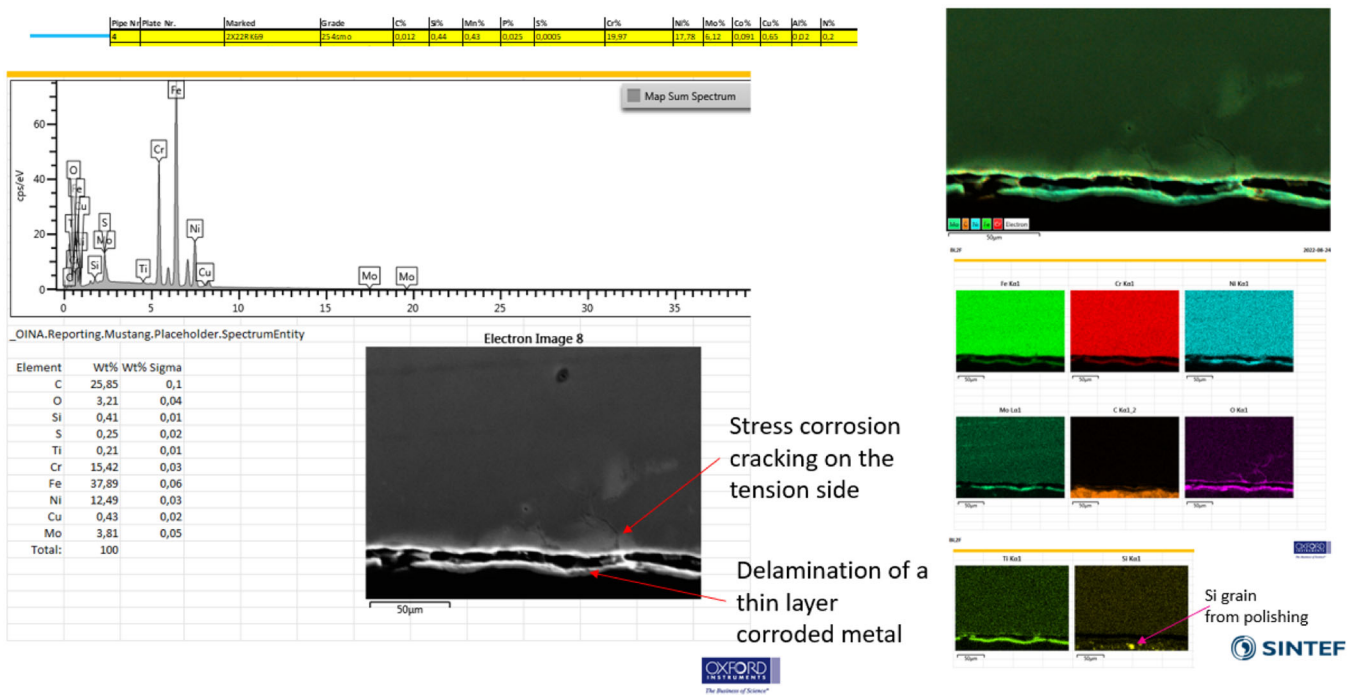

FIGURE 9 Posttest SEM/EDS element mapping of 254SMO revealing SCC and a thin delaminated metal/oxide layer on the stressed surface. EDS, energy dispersive X-ray spectroscopy; SCC, stress corrosion cracking; SEM, scanning electron microscopy. [Color figure can be viewed at wileyonlinelibrary.com]

Also, on the mid-section of the C-ring, general corrosion was seen.

In the SEM/EDS elements mapping, SCC along the grain boundaries with lost grains is seen. The Al intensity is somewhat higher in the grain boundaries (see Figure 15). This could come from the 2.2 wt% Al-alloy itself, but also from precipitation of the partly dissolved alumina spacers.

A selective dissolution (dealloying) of essential alloying elements (Ni, Mo, and Fe) has been observed in the supercritical region for certain Ni-based superalloys. A subsequent transformation of metal into a scale is accompanied by a reduction in the wall thickness. Intergranular grain attack (corrosion) precedes the dissolving of alloying elements and causes sub-surface damage.[10]
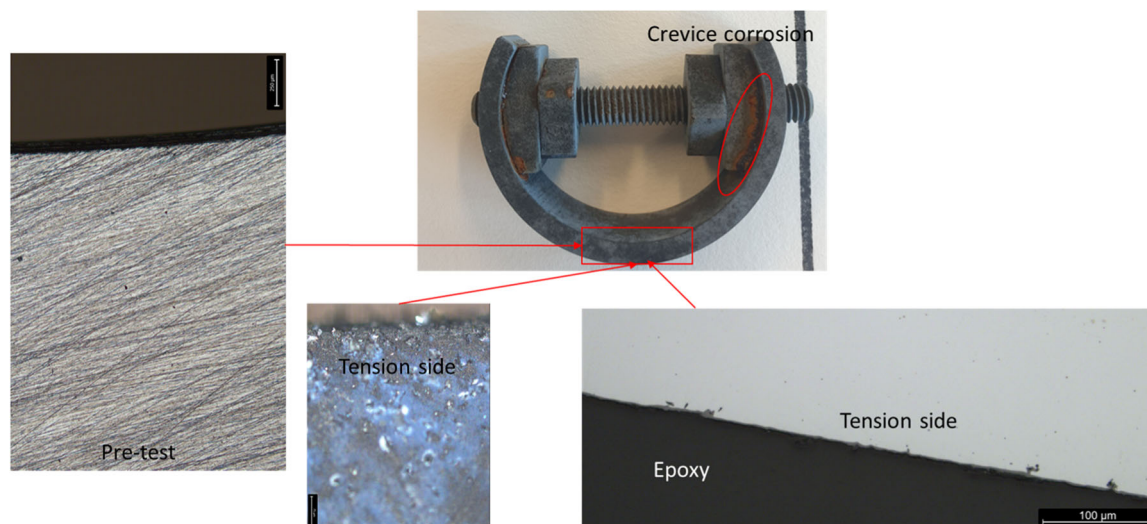
FIGURE 10 Posttest analysis of P91 performed with optical microscopy of sections. [Color figure can be viewed at wileyonlinelibrary.com]
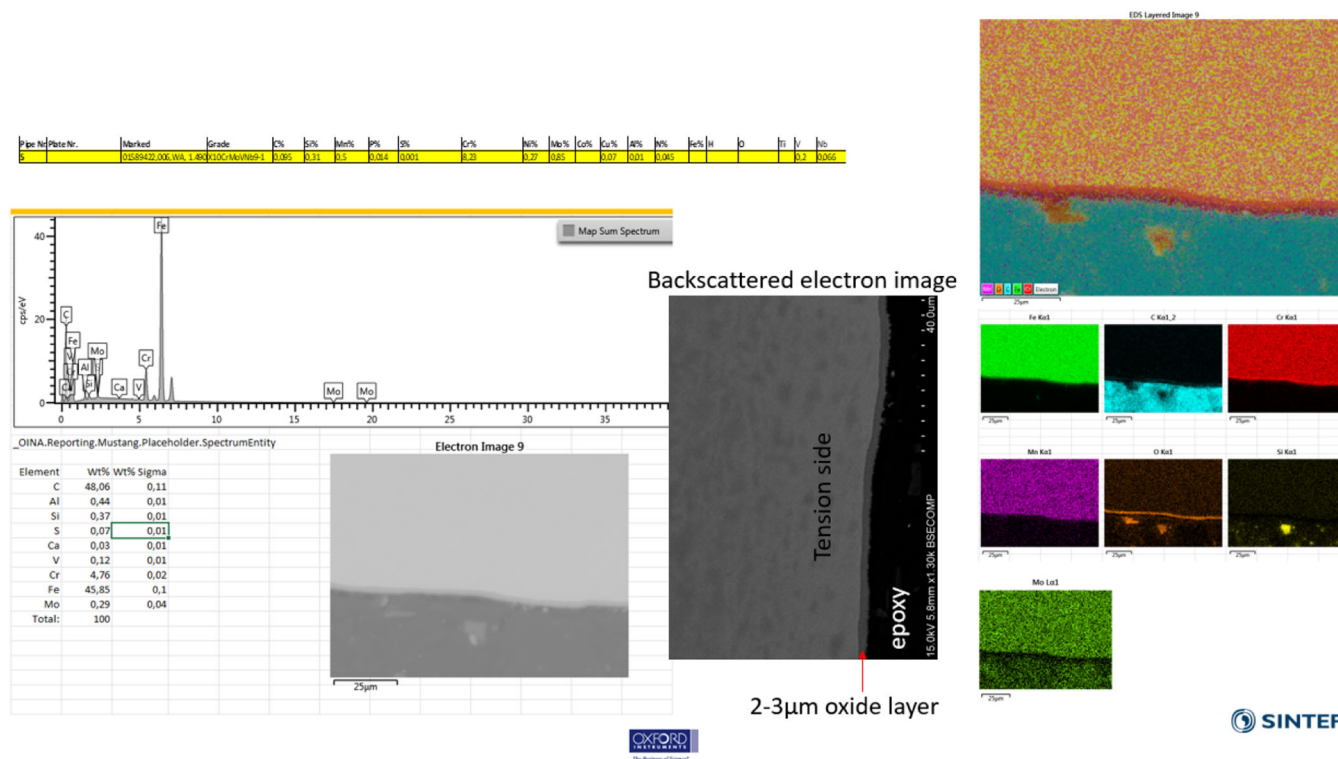

FIGURE 11 In the SEM/EDS mapping, it is seen that the oxide layer is richer in Cr compared to the substrate on the exposed P91 samples. EDS, energy dispersive X-ray spectroscopy; SEM, scanning electron microscopy. [Color figure can be viewed at wileyonlinelibrary.com]

4 | DISCUSSION

There is neither much literature nor experience available on corrosion in black liquor process systems operating at supercritical conditions. Most data apply for 100–200°C, that is, not supercritical.[11] Hence, it has been aimed to investigate the behavior of certain commercial steel qualities at supercritical conditions as a basis for the construction of a small-scale pilot system.

In general, it is known that the presence of chlorides, hydroxides, sulfides, and certain wood extractives increases the corrosivity of black liquor.[12] This can result in the weakening of the protective passive film (i.e., corrosion) on carbon steels and cause
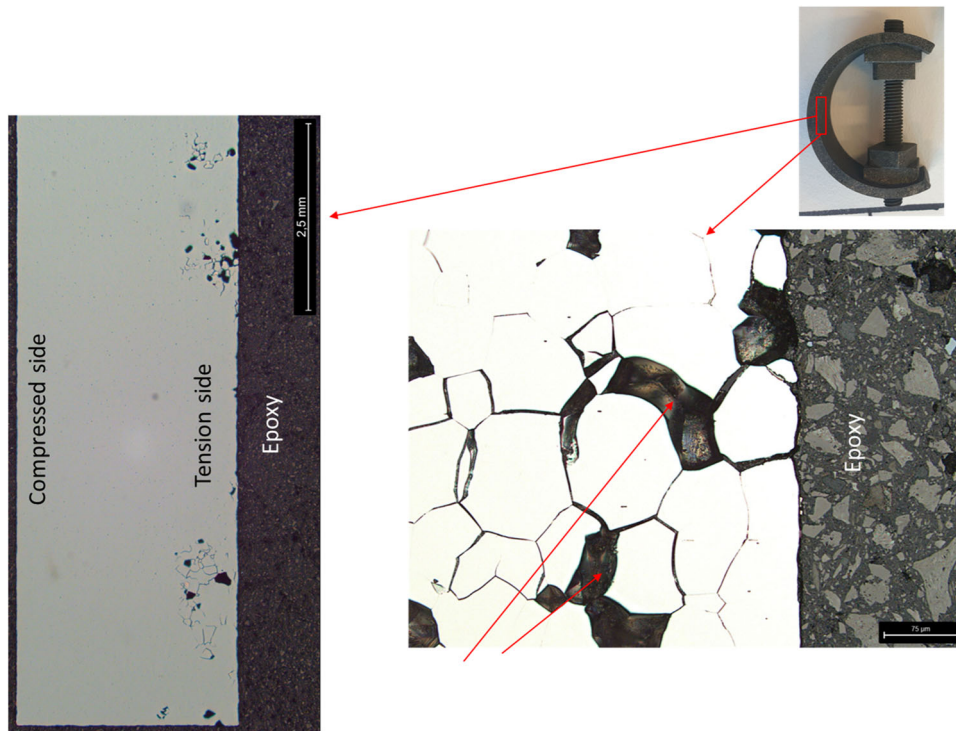
FIGURE 12 Optical microscopy images of as-tested C-276 C-rings. The loss of some grains is seen because of the combination of applied stress and corrosion. [Color figure can be viewed at wileyonlinelibrary.com]
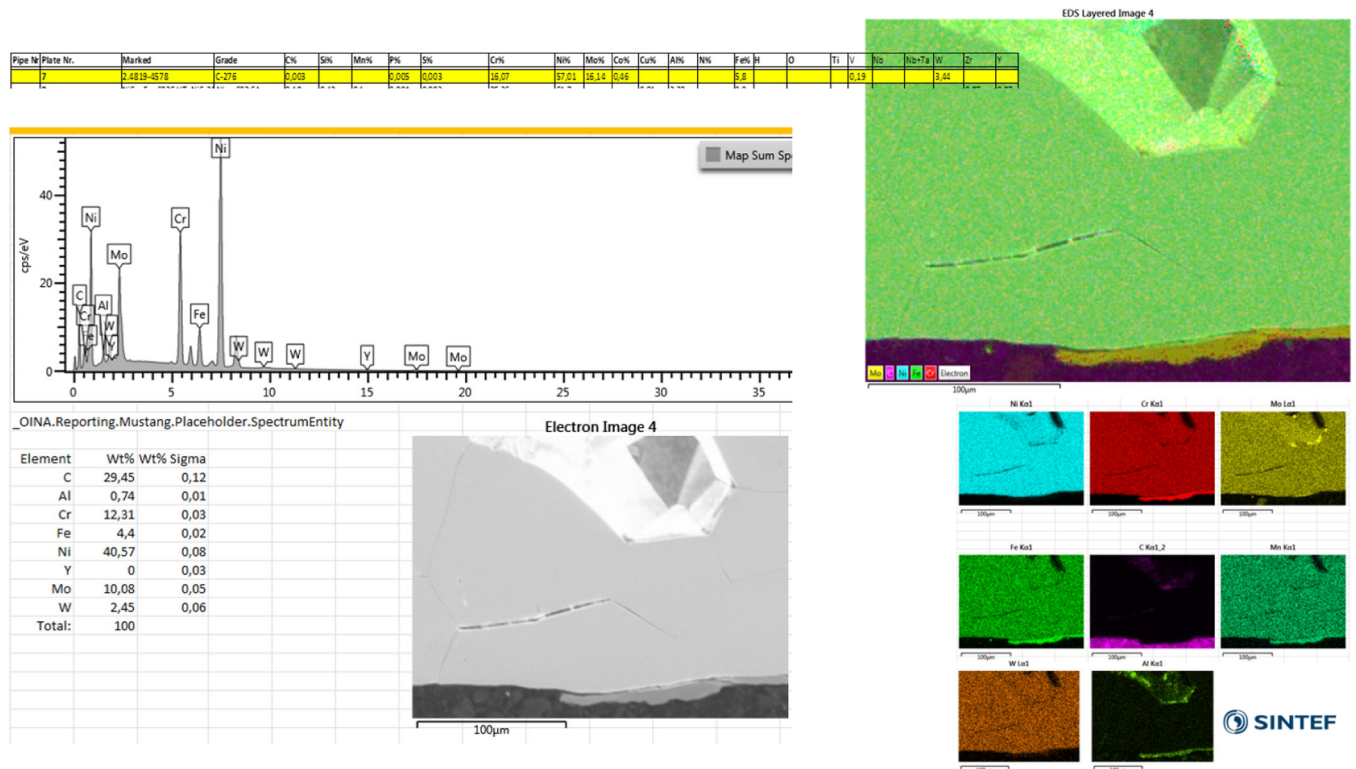

FIGURE 13 SEM/EDS mapping of C-276 showing SCC with dropped-out grains. EDS, energy dispersive X-ray spectroscopy; SCC, stress corrosion cracking; SEM, scanning electron microscopy. [Color figure can be viewed at wileyonlinelibrary.com]
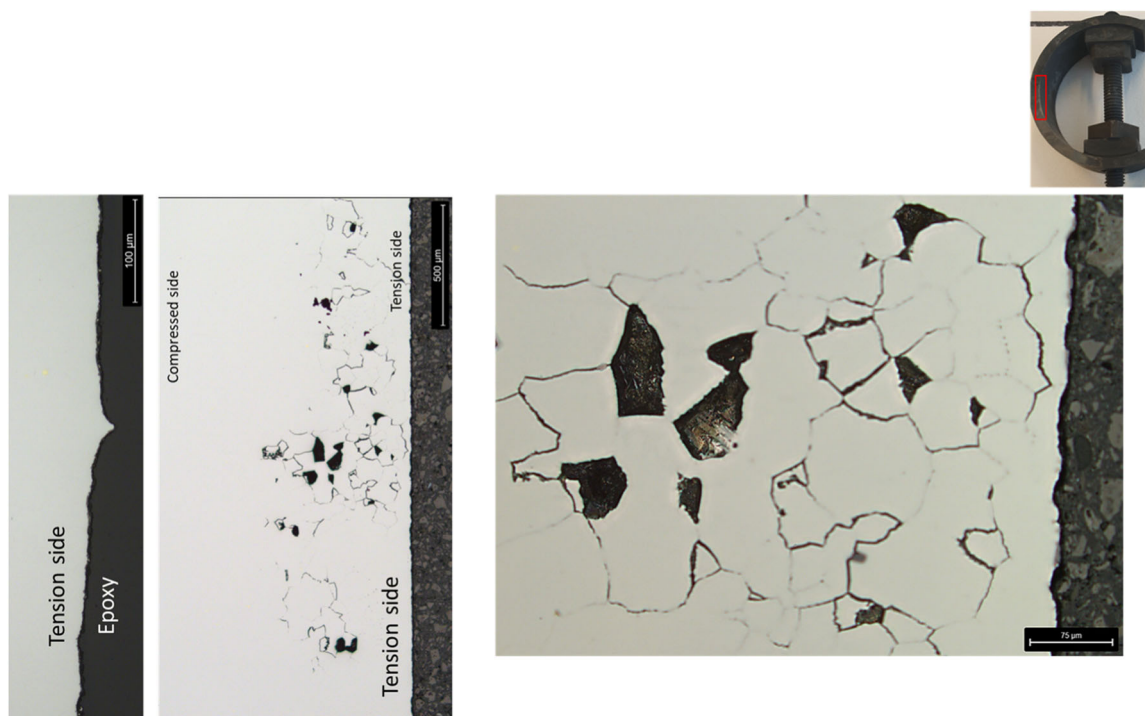
FIGURE 14 Optical microscopy images of sections of the 699XA NiCr alloy with Al as tested revealing general corrosion and lost grains on the tension side due to SCC. SCC, stress corrosion cracking. [Color figure can be viewed at wileyonlinelibrary.com]
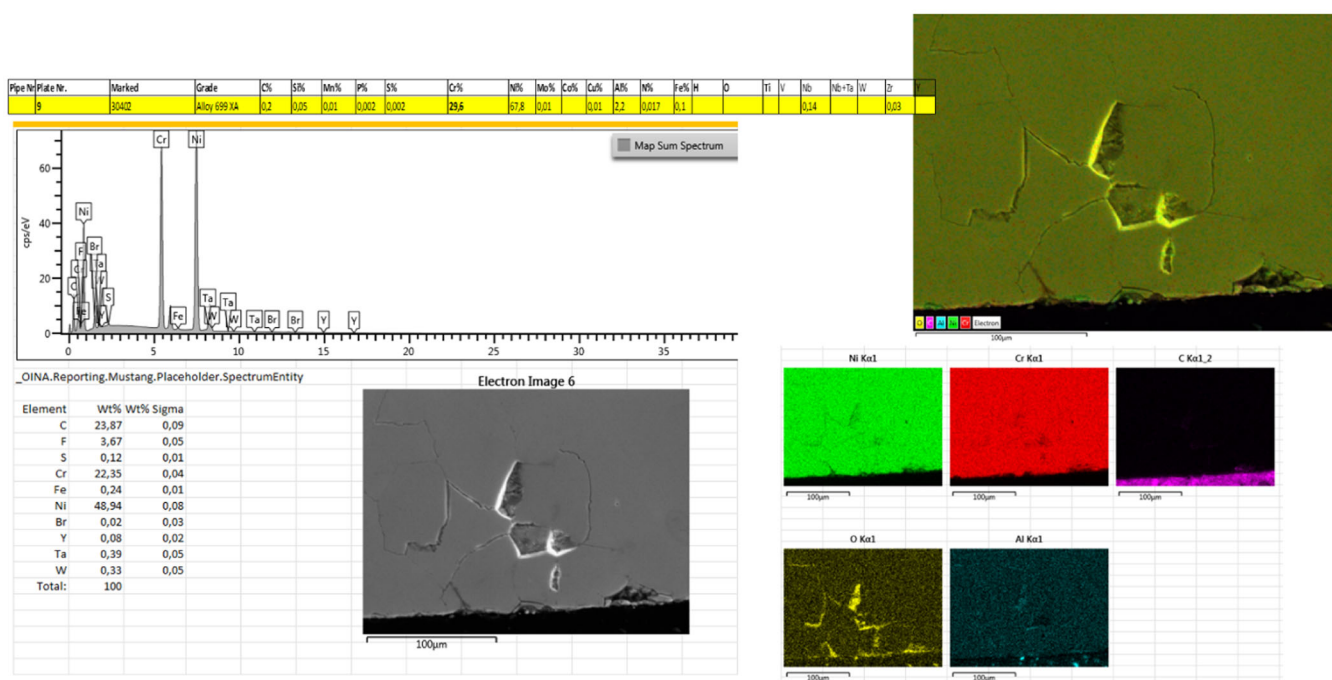

FIGURE 15 SEM/EDS element mapping of 699XA exposed to super critical conditions. EDS, energy dispersive X-ray spectroscopy; SEM, scanning electron microscopy. [Color figure can be viewed at wileyonlinelibrary.com]

cracking in stainless qualities. More information can be found in the literature.[11] However, these results apply to non-supercritical conditions and cannot uncritically be considered as applicable to supercritical conditions

as well, a condition in which the properties of the vapor and the gas phase behave quite differently, affecting the solubility of protective passive films (e.g., carbonate). Liu et al. report high corrosion rates of P91 in acidic

media under stagnant conditions. However, the corrosion rate is acceptable at HTL conditions with higher pH.[5]

It is also an important point that most non-supercritical laboratory tests reported in the literature have been conducted in real black liquor containing oil components forming a protective layer on the exposed steel surfaces. This can result in nonconservative results as it is quite normal that water and oil separate under laminar flow conditions resulting in steel surfaces not being covered with an oil film. As a result, severe corrosion may take place at locations wetted with supercritical water containing chlorides, sulfides, and so on.

A selective dissolution (dealloying) of essential alloying elements (Ni, Mo, and Fe) has been observed in the supercritical region for certain Ni-based superalloys. A subsequent transformation of metal into a scale is accompanied by a reduction in the wall thickness. IG attack precedes the dissolving of alloying elements and causes sub-surface damage.[10]

Also, Liu et al. state that the average corrosion rate of P91 in a stagnant catalytic HTL environment falls under a proposed corrosion allowance of 0.1 mm/year for a 20-year life span[5]. The results reported herein should be considered as indicative only until further tests have been carried out on the P91 "winner candidate" in the welded condition. This is important as it is a well-known fact that welds always reduce the resistivity to corrosion for most materials due to grain coarsening, chromium depletion, intercrystalline carbide formation, residual stresses, undercuts/defects, poor post-welding pickling, and so on.

5 | CONCLUSIONS

As of September 2022, the corrosion and material evaluation study in (a) water-based simulated black liquor and (b) water-based simulated black liquor at super-critical conditions was successful. The conclusion from the testing program was that the most CRA for the defined conditions is the chromium-rich carbon steel candidate P91 (UNS K91560). This is a type of creep strength-enhanced ferritic alloy, which are steels designed to retain strength at high temperatures. The P91 abbreviation represents the material's chemical composition, that is, 9% chromium (Cr) and 1% molybdenum (Mo). Further work is required to conclude on corrosion resistance for the P91 quality at supercritical conditions in the welded conditions and to better understand caustic corrosion and cracking mechanisms.

AUTHOR CONTRIBUTIONS

All authors contributed to the conceptualization of this work. The corrosion testing methodology was outlined by

Torstein Lange and Daniel Blücher. The validation was performed by Torstein Lange, Daniel Blücher, Judit Sandquist, and Inge Saanum. The analysis and writing were performed by all authors.

CONFLICT OF INTEREST STATEMENT
The authors declare no conflict of interest.

DATA AVAILABILITY STATEMENT
The data that support the findings of this study are openly available in Black Liquor to Fuel at https://wiki.eduuni.fi/x/XSrNC.

ORCID
Daniel Blücher http://orcid.org/0000-0002-5669-7535

REFERENCES
[1] R. Morya, M. Kumar, I. Tyagi, A. Kumar Pandey, J. Park, T. Raj, R. Sirohi, V. Kumar, S. H. Kim, *Bioresour. Technol.* **2022**, *350*, 126916.
[2] http://www.bl2f.eu
[3] L. Grande López, I. Pedroarena Apezteguía, S. A. Korili, A. Gil Bravo, *Materials* **2021**, *14*, 18.
[4] N. Ghavami, K. Özdenkçi, G. Salierno, M. Björklund-Sänkiaho, C. De Blasio, *Biomass Convers. Biorefin.* **2021**, *13*, 12367.
[5] M. Liu, Y. Zeng, J. L. Luo, *Corros. Sci.* **2023**, *218*, 111148.
[6] ANSI/NACE TM0177. Item No. 21212, Laboratory Testing of Metals for Resistance to Sulfide Stress Cracking and Stress Corrosion Cracking in H2S Environments **2016**.
[7] W. Moss, *Guidelines on Materials Requirements for Carbon and Low Alloy Steels: For H2S-Containing Environments in Oil and Gas Production*, CRC Press, London **2019**.
[8] P. R. Rhodes, *Corrosion* **2001**, *57*, 923.
[9] https://norbiolab.no/list-of-infrastructure/continuous-htl-processing-reactor
[10] W. Habicht, N. Boukis, E. Hauer, E. Dinjus, *X-Ray Spectrom.* **2011**, *40*, 69.
[11] L. Esteves, M. Cardoso, V. D. F. C. Lins, *Mater. Res.* **2017**, *21*, 1.
[12] H. Sarmiento Klapper, J. Klöwer, O. Gosheva, *Philos. Trans. R. Soc. A* **2017**, *375*, 20160415.